SUPPORTING INFORMATION

Acidity and nucleophilic reactivity of glutathione persulfide

Dayana Benchoam[1,2,‡], Jonathan A. Semelak[3,‡], Ernesto Cuevasanta[1,2,4], Mauricio Mastrogiovanni[2,5], Juan S. Grassano[3], Gerardo Ferrer-Sueta[2,6], Ari Zeida[2,5], Madia Trujillo[2,5], Matías N. Möller[2,6,*], Darío A. Estrin[3,*], and Beatriz Alvarez[1,2,*]

[1]Laboratorio de Enzimología, Instituto de Química Biológica, Facultad de Ciencias, Universidad de la República, Montevideo 11400, Uruguay

[2]Centro de Investigaciones Biomédicas (CEINBIO), Universidad de la República, Montevideo 11800, Uruguay

[3]Departamento de Química Inorgánica, Analítica y Química Física, INQUIMAE-CONICET, Facultad de Ciencias Exactas y Naturales, Universidad de Buenos Aires, Ciudad Universitaria, Pabellón 2, Buenos Aires 1428, Argentina

[4]Unidad de Bioquímica Analítica, Centro de Investigaciones Nucleares, Facultad de Ciencias, Universidad de la República, Montevideo 11400, Uruguay

[5]Departamento de Bioquímica, Facultad de Medicina, Universidad de la República, Montevideo 11800, Uruguay

[6]Laboratorio de Fisicoquímica Biológica, Instituto de Química Biológica, Facultad de Ciencias, Universidad de la República, Montevideo 11400, Uruguay

‡These authors contributed equally.

*Corresponding authors: M.N. Möller, D.A. Estrin, B. Alvarez

E-mails: mmoller@fcien.edu.uy, dario@qi.fcen.uba.ar, beatriz.alvarez@fcien.edu.uy

Running title: Acidity and nucleophilicity of glutathione persulfide

List of supplemental materials:

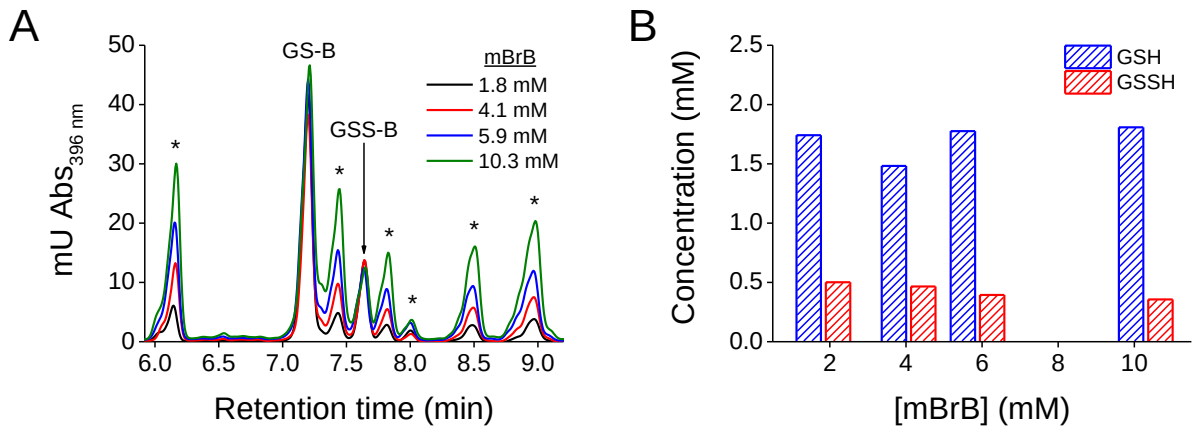

Figure S1. Quantification of GSH and GSSH derivatized with increasing concentrations of mBrB. A mixture of GSSG (3 mM) and H_2S (3 mM) was incubated in phosphate buffer (0.1 M, pH 7.4, 0.1 mM dtpa) at 25 °C for 35 min. Then, aliquots were 15-fold diluted in the presence of mBrB (1.8-10.3 mM, final concentrations). **A.** Reversed-phase HPLC of the samples. The asterisks represent contaminants present in mBrB. **B.** Concentrations of GSH (blue) and GSSH (red) in the mixture derivatized with different concentrations of mBrB. Minimum differences in the detected GSH and GSSH can be explained by the baseline shift that occurs when the concentration of mBrB increases.

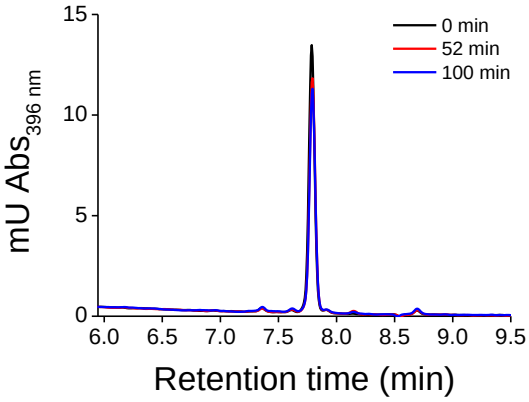

Figure S2. Stability of GSS-B. A mixture of GSSG (9 mM) and H_2S (0.5 mM) in phosphate buffer (0.1 M, pH 7.4), was incubated at 25 °C for 2 h and derivatized with mBrB (4 mM). The mixture was injected in the reversed-phase HPLC and the peak corresponding to GSS-B (retention time 7.7 min) was collected. Aliquots of the collected peak were re-injected immediately, after 52 min, and after 100 min at 25 °C.

Table S1. Computed Gibbs energy changes (kcal/mol) of the processes involved in the proton dissociation of MeSH and MeSSH by means of electronic structure methods and PCM solvation models.

XH	Method	XH and H_2O desolvation[a]	X-H bond cleavage[b]	$X^{\bullet}$ electron affinity and hydrogen ionization[c]	H_2O proton affinity[d]	X^- and H_3O^+ solvation[e]	Global process[f]
MeSH	PBE/dzvp	7.7	73.5	277.5	-156.4	-146.3	56.0
	MP2/dzvp	8.6	64.1	285.5	-153.6	-146.2	58.4
	ωB97x-D/6-31 G(d')	8.0	73.6	283.2	-164.4	-147.1	53.3
	M062X/6-31 G(d')	7.9	75.5	277.5	-162.3	-146.6	52.0
	CCSD/6-31 G(d')	8.1	65.0	293.4	-163.5	-145.4	57.6
MeSSH	PBE/dzvp	7.9	56.4	278.9	-156.4	-140.5	46.3
	MP2/dzvp	8.9	51.2	283.0	-153.6	-140.7	48.8
	ωB97x-D/6-31 G(d')	8.3	59.9	280.6	-164.4	-141.6	42.8
	M062X/6-31 G(d')	8.1	59.9	276.8	-162.3	-141.1	41.4
	CCSD/6-31 G(d')	8.4	52.3	290.3	-163.5	-139.8	47.7
Relative difference MeSH-MeSSH	CCSD/6-31 G(d')	-3.7 %	19.5 %	1.1 %	N/A	3.9 %	17.2 %

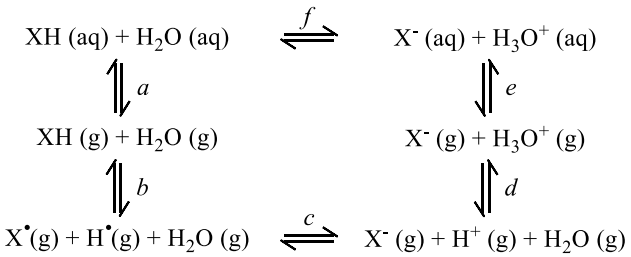

Table S2. pH-dependency of the apparent rate and equilibrium constants of Reaction 1.

	Reacting species	Rate or equilibrium constant at pH 7.4	Equation[a,b]
k_1	HS^- + GSSG	0.23 M^{-1} s^{-1}	$k_{1,pH} = k_{1,ind} \frac{K_a^{H_2S}}{K_a^{H_2S} + [H^+]}$
k_{-1}	GS^- + GSSH	1.11 M^{-1} s^{-1}	$k_{-1,pH} = k_{-1,ind} \frac{K_a^{GSH}}{K_a^{GSH} + [H^+]} \frac{[H^+]}{K_a^{GSSH} + [H^+]}$
K_{eq1}	HS^- + GSSG GS^- + GSSH	0.194	$K_{eq1,pH} = K_{eq1,ind} \frac{K_a^{H_2S} (K_a^{GSH} + [H^+])(K_a^{GSSH} + [H^+])}{(K_a^{H_2S} + [H^+]) K_a^{GSH} [H^+]}$

[a] pK_as: H_2S, 6.98 (1); GSH, 8.94 (2); GSSH, 5.45.

[b] k_{pH} and $K_{eq,pH}$ refer to the apparent rate and equilibrium constants, respectively, at a particular pH, *e.g.* 7.4; k_{ind} and $K_{eq,ind}$ are the pH-independent rate and equilibrium constants, respectively, *i.e.* the constants corresponding to the protonation states adequate for reaction.

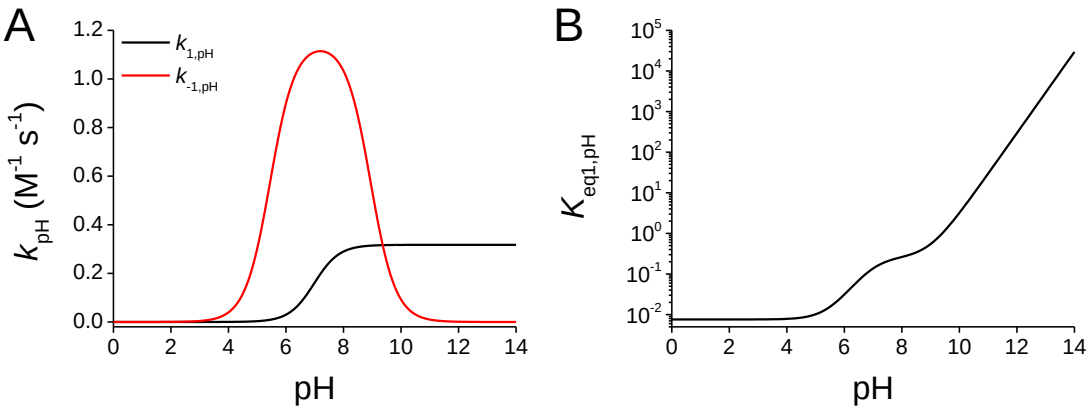

Figure S3. Dependence of apparent kinetic and equilibrium constants of Reaction 1 with pH. A. pH profile for $k_{1,pH}$ (HS^- + GSSG, $k_{pH\ 7.4}$ = 0.23 M^{-1} s^{-1}) and $k_{-1,pH}$ (GS^- + GSSH, $k_{pH\ 7.4}$ = 1.11 M^{-1} s^{-1}); $k_{1,pH}$ (black) increases as the pH increases owing to the higher availability of the ionized species (HS^-), while $k_{-1,pH}$ (red) presents a bell shaped profile, since one species needs to be deprotonated (GS^-) and the other one protonated (GSSH) for the reaction to occur. **B.** pH profile for $K_{eq1,pH}$.

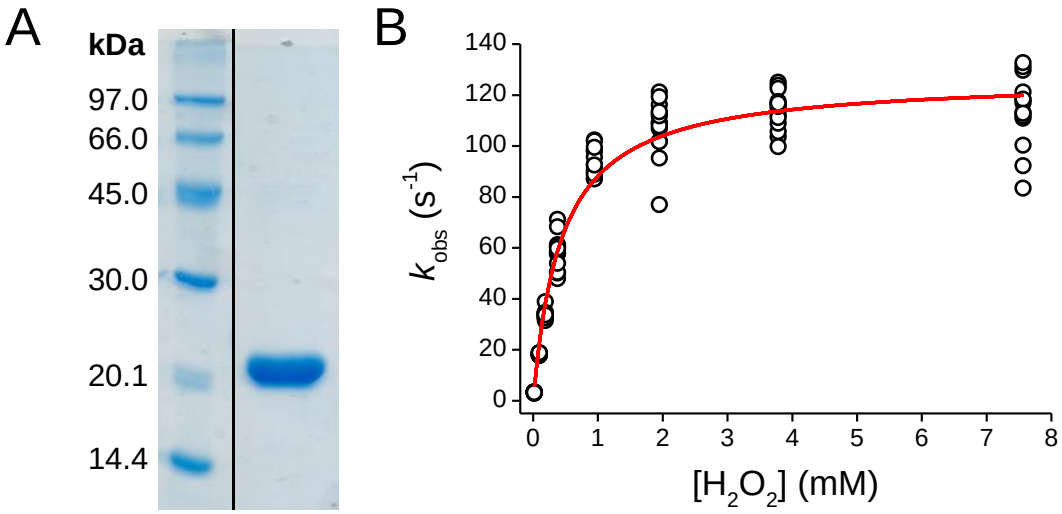

C

Nominal mass (M_r): **21460**; Calculated pI value: **6.75**

Variable modifications: Oxidation (M)
Cleavage by Trypsin: cuts C-term side of KR unless next residue is P
Sequence Coverage: **91%**

Matched peptides shown in **Bold Red**

```
  1  MGSSHHHHHH SSGLVPRGSH MAPIKVGDAI PAVEVFEGEP GNKVNLAELF
 51  KGKKGVLFGV PGAFTPGCSK THLPGFVEQA EALKAKGVQV VACLSVNDAF
101  VTGEWGRAHK AEGKVRLLAD PTGAFGKETD LLLDDSLVSI FGNRRLKRFS
151  MVVQDGIVKA LNVEPDGTGL TCSLAPNIIS QLLEDPAANK ARKEAELAAA
201  TAEQ
```

Figure S4. **Characterization of the peroxiredoxin Prx5 variant (Prx5v) used for H_2O_2 quantification.** The coding sequence of human Prx5 (GenBank accession number: NM_012094NM_001202431) was synthesized and cloned into a pET-15b vector with NdeI and XhoI by Genescript. The plasmid includes a N-terminal 6×His-Tag and thrombin site which results in 21 additional residues. The coding sequence also included 22 extra residues in the C-terminal end. Prx5v was expressed in *Escherichia coli* and purified as previously described (3). **A.** The protein migrated as a single band in SDS-PAGE. **B.** The kinetics of the reaction of reduced protein (0.5 µM) in acetic/MES/tris buffer, pH 7.1, 25 °C towards H_2O_2 (0.02-7.5 mM) was studied by the increase in intrinsic fluorescence (λ_{ex} = 280 nm, emission cut-off 320 nm) in a stopped-flow spectrofluorimeter. As in the case of the wild-type protein, the plot of k_{obs} *versus* H_2O_2 concentration was hyperbolic (2, 4). From the plot, a second-order rate constant of reaction with H_2O_2 to form sulfenic acid was calculated to be $(2.9 \pm 0.7) \times 10^5$ M^{-1} s^{-1}, similar to that of the wild type, 3.0×10^5 M^{-1} s^{-1} (pH 7.4, 25 °C) (4), 4.3×10^5 M^{-1} s^{-1} (pH 6.9, 25 °C) (2). The plateau, which can be interpreted to represent disulfide formation from sulfenic acid and the resolving cysteine (4), had a value of 127 ± 2 s^{-1}. This is higher than that of the wild type, 14.7 s^{-1} (pH 7.4, 25 °C) (4), 21 s^{-1} (pH 6.9, 25 °C) (2), thus, Prx5v minimizes parallel reactions of the sulfenic acid. **C.** The sequence of the protein was verified by MALDI-TOF MS and MS/MS of tryptic fragments, with 91 % coverage. MALDI-TOF experiments were performed in the facility of the Institut Pasteur de Montevideo, Uruguay.

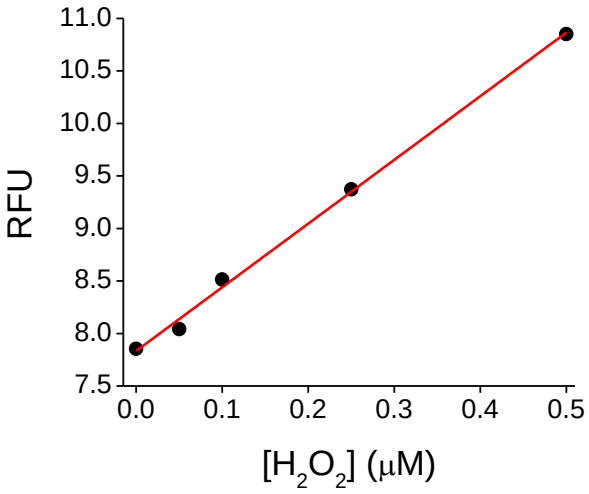

Figure S5. Calibration curve of H_2O_2 with reduced Prx5v. H_2O_2 (0-0.5 μM) was exposed to reduced Prx5v (2 μM) in phosphate buffer (50 mM, pH 7.4, 0.1 mM dtpa). The fluorescence increase (λ_{ex} = 280 nm, λ_{em} = 340 nm) was measured at 25 °C.

Table S3. Gibbs energy barriers ($\Delta G^{\ddagger}$, kcal/mol) for the reactions of MeS^- or $MeSS^-$ with mBrB, ONOOH, and H_2O_2 obtained from umbrella sampling-QM/MM Gibbs energy profiles (level of theory PBE/dzvp) and comparison with values estimated from experimental measurements.

	Gibbs energy profiles			Estimated[a]		
	$\Delta G^{\ddagger}$ MeS^-	$\Delta G^{\ddagger}$ $MeSS^-$	$\Delta\Delta G^{\ddagger}$[b]	$\Delta G^{\ddagger}$ GS^-	$\Delta G^{\ddagger}$ GSS^-	$\Delta\Delta G^{\ddagger}$[b]
mBrB	6.5 ± 0.6	4.4 ± 0.3	2.1 ± 0.9	14.3	12.1	2.2
ONOOH	2.7 ± 0.3	2.5 ± 0.5	0.2 ± 0.8	10.6	10.1	0.5
H_2O_2	6.7 ± 0.4	5.7 ± 0.4	1.0 ± 0.8	15.4	16.2	-0.8

[a] Estimated from the experimental k_{ind} for GS^- and GSS^- according to the Transition State Theory, $k = \frac{\tau k_B T}{hC^o} e^{-\Delta G^{\ddagger}/RT}$ (R, ideal gas constant; T, temperature; k_B and h, Boltzmann and Plank constants; $C°$, 1 M; τ, transmission coefficient).

[b] Values of $\Delta\Delta G^{\ddagger}$ correspond to $\Delta G^{\ddagger}_{thiolate} - \Delta G^{\ddagger}_{persulfide.}$

Table S4. Thermodynamic properties (kcal/mol) for MeS^- and $MeSS^-$ reactions towards ONOOH and H_2O_2, both *in vacuo* and with PCM solvated species.

Method	MeS^- + ONOOH		$MeSS^-$ + ONOOH		$\Delta\Delta G^a$	
	$\Delta G^‡$	ΔG_{reac}	$\Delta G^‡$	ΔG_{reac}	$\Delta\Delta G^‡$	$\Delta\Delta G_{reac}$
PBE/dzvp/*in vacuo*	4.1	-39.9	1.8	-42.8	2.3	2.9
MP2/dzvp/*in vacuo*	15.6	-57.5	12.4	-56.9	3.2	-0.6
ω*B97x-D/6-31 G(d')/*in vacuo	14.5	-45.5	10.5	-47.5	4.1	2.0
M062X/6-31 G(d')/*in vacuo*	16.2	-48.4	12.5	-49.2	3.7	0.8
PBE/dzvp/PCM	3.2	-43.7	2.5	-44.1	0.7	0.4
MP2/dzvp/PCM	14.6	-61.0	9.7	-59.7	5.0	-1.3
***ω*B97x-D/6-31 G(d')/PCM**	12.8	-48.8	10.2	-47.7	2.6	-1.1
M062X/6-31 G(d')/PCM	14.9	-50.9	11.4	-49.4	3.5	-1.4
Method	MeS^- + H_2O_2		$MeSS^-$ + H_2O_2		$\Delta\Delta G^a$	
	$\Delta G^‡$	ΔG_{reac}	$\Delta G^‡$	ΔG_{reac}	$\Delta\Delta G^‡$	$\Delta\Delta G_{reac}$
PBE/dzvp/*in vacuo*	12.5	-33.8	9.5	-42.2	3.0	8.4
MP2/dzvp/*in vacuo*	20.3	-43.1	18.4	-47.8	1.9	4.7
ω*B97x-D/6-31 G(d')/*in vacuo	25.2	-30.7	24.2	-34.2	1.0	3.5
M062X/6-31 G(d')/*in vacuo*	28.6	-31.5	27.9	-33.8	0.7	2.3
PBE/dzvp/PCM	8.4	-39.7	7.5	-44.1	0.9	4.4
MP2/dzvp/PCM	15.6	-49.4	15.2	-50.5	0.4	1.1
***ω*B97x-D/6-31 G(d')/PCM**	20.6	-35.3	20.9	-36.0	-0.3	0.7
M062X/6-31 G(d')/PCM	23.8	-36.4	23.1	-36.4	0.7	0.0

[a] Values of $\Delta\Delta G$ correspond to $\Delta G_{thiolate} - \Delta G_{persulfide}$.

Table S5. Evolution of Mulliken charges (*e*) for the reactions of MeS^- or $MeSS^-$ with mBrB, ONOOH, and H_2O_2 obtained from umbrella sampling-QM/MM Gibbs energy profiles[a].

	mBrB		ONOOH		H_2O_2	
	MeS^-	$MeSS^-$	MeS^-	$MeSS^-$	MeS^-	$MeSS^-$
Reactant complex	-0.97	-0.99	-0.84	-0.86	-0.85	-0.90
Transition state	-0.60	-0.57	-0.74	-0.72	-0.68	-0.70
Product complexes	0.09	0.01	0.14	0.18	0.20	0.20
% Charge transferred in the transition state	38	42	12	16	20	22

[a] Average values were computed from windows centered in each reaction stage.

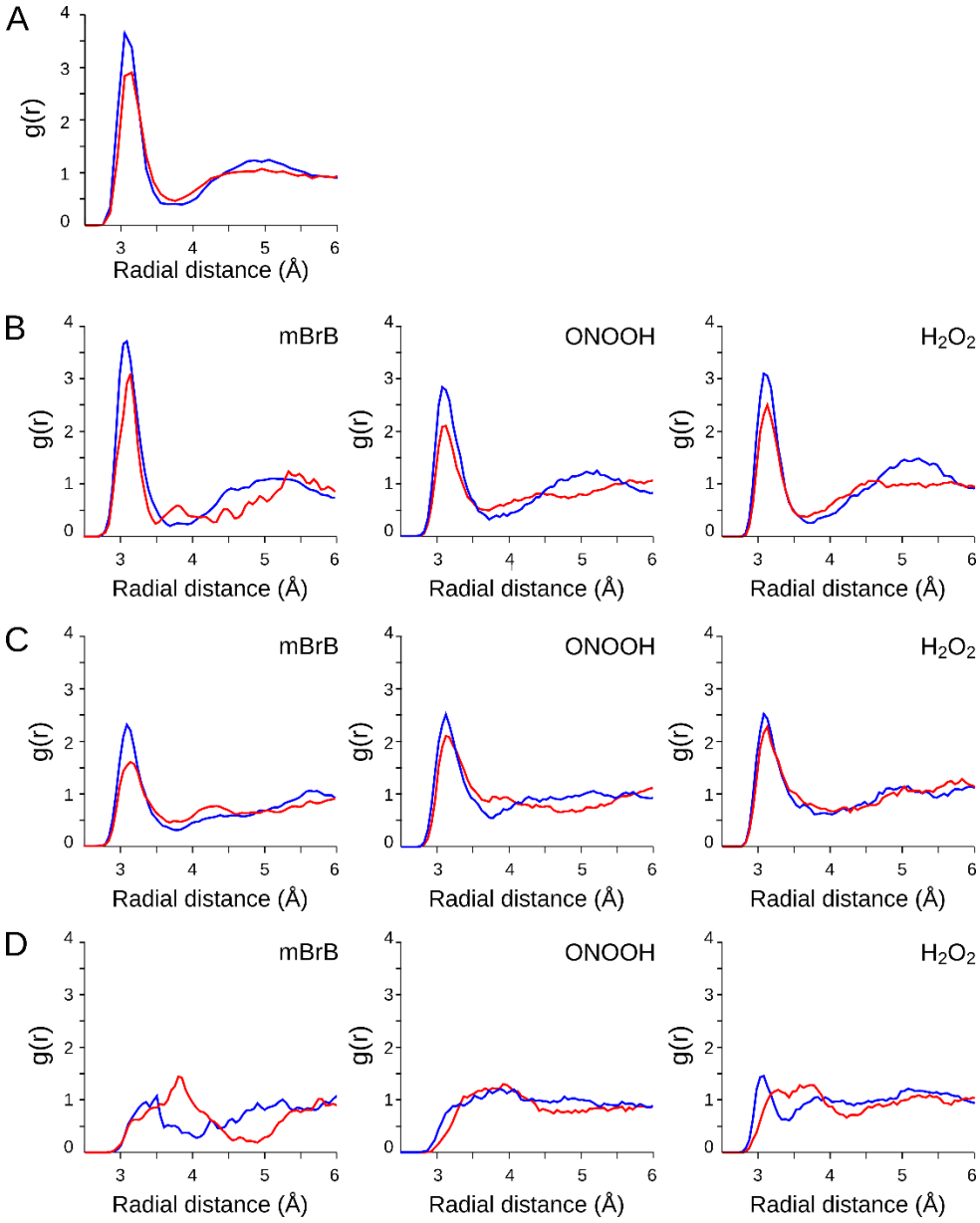

Figure S6. Evolution of solvation patterns of the reactions of MeS^- and $MeSS^-$ with mBrB, ONOOH, and H_2O_2. Radial correlation function centered on the nucleophilic sulfur atoms of MeS^- (blue) and $MeSS^-$ (red), computed from a 50 ps long QM/MM MD with the stochastic Langevin thermostat. **A.** Free reactant, **B,** reactant complex, **C,** transition state, and **D,** product complex.

References

1. Hughes, M. N., Centelles, M. N., and Moore, K. P. (2009) Making and working with hydrogen sulfide: The chemistry and generation of hydrogen sulfide in vitro and its measurement in vivo: a review. *Free Radic. Biol. Med.* **47**, 1346–1353
2. Portillo-Ledesma, S., Sardi, F., Manta, B., Tourn, M. V., Clippe, A., Knoops, B., Alvarez, B., Coitiño, E. L., and Ferrer-Sueta, G. (2014) Deconstructing the catalytic efficiency of peroxiredoxin-5 peroxidatic cysteine. *Biochemistry*. **53**, 6113–6125
3. Declercq, J. P., Evrard, C., Clippe, A., Stricht, D. V., Bernard, A., and Knoops, B. (2001) Crystal structure of human peroxiredoxin 5, a novel type of mammalian peroxiredoxin at 1.5 Å resolution. *J. Mol. Biol.* **311**, 751–759
4. Trujillo, M., Clippe, A., Manta, B., Ferrer-Sueta, G., Smeets, A., Declercq, J.-P., Knoops, B., and Radi, R. (2007) Pre-steady state kinetic characterization of human peroxiredoxin 5: taking advantage of Trp84 fluorescence increase upon oxidation. *Arch. Biochem. Biophys.* **467**, 95–106